Journal of Catalysis **202,** 402–412 (2001)
doi:10.1006/jcat.2001.3294, available online at http://www.idealibrary.com on IDEAL®

Ethylbenzene Isomerization on Bifunctional Platinum Alumina–Mordenite Catalysts

1. Influence of the Mordenite Si/Al Ratio

F. Moreau,* S. Bernard,* N. S. Gnep,* S. Lacombe,† E. Merlen,† and M. Guisnet*,[1]

*Catalyse en Chimie Organique, Faculté des Sciences, UMR 6503, 40, avenue du Recteur Pineau, 86022 Poitiers Cedex, France; and †Institut Français du Pétrole, 1 et 4, avenue de Bois-Préau, 92852 Rueil-Malmaison Cedex, France

Received March 27, 2001; revised May 21, 2001; accepted May 21, 2001

The transformation of ethylbenzene was carried out on intimate mixtures of 0.5 wt% Pt/Al_2O_3 (75 wt%) with a platinum dispersion of 100% and of HMOR zeolites (25 wt%) with Si/Al ratios between 6.6 and 180. Products result from six main transformations of ethylbenzene or/and of the reaction products: the desired isomerization of ethylbenzene into xylenes (reaction 1), disproportionation of ethylbenzene (2), dealkylation followed by hydrogenation of ethylene (3), secondary ethylbenzene–xylene transalkylation (4), hydrogenation of ethylbenzene followed by ethylcyclohexane isomerization (5), and secondary cracking of C_8 naphthenes (6). From the comparison of the product distributions over Pt/Al_2O_3, over HMOR and over the bifunctional catalysts, reactions 2–4 were confirmed to occur through acid catalysis and hydrogenation through metal catalysis, and reactions 1 and 6 through bifunctional catalysis. Whatever the catalyst, the selectivity to isomers increases with ethylbenzene conversion, which is due to thermodynamic limitations in reactions 2 and 5. A significant increase in selectivity to isomers is also observed when the Si/Al ratio of the mordenite component increases from 20 to 180. With these bifunctional catalysts, the initial rate of disproportionation is proportional to the square of the concentration of protonic sites, which suggests that this bimolecular reaction requires two protonic sites for its catalysis; furthermore, the rate of dealkylation (per protonic site) depends only on the strength of the protonic sites and the change of the isomerization rate with the balance between the metallic and acidic functions is the one expected from a classical bifunctional mechanism. For the bifunctional catalysts with HMOR6.6 and −10 as acidic components, the rates of disproportionation, dealkylation, and isomerization are lower than expected and the selectivity to isomers is higher. This can be explained by strong diffusion limitations in these zeolites which, in contrast to the other samples, do not present mesopores in addition to micropores.

Key Words: **ethylbenzene isomerization; disproportionation; Pt; mordenite; Si/Al ratio.**

INTRODUCTION

The C_8 aromatic fraction which is obtained from steam cracking and especially from naphtha reforming is constituted by the mixture of xylenes at thermodynamic equilibrium, i.e., approximately 25% of para, 25% of ortho, and 50% of meta, together with approximately 20% and 50% ethylbenzene in the C_8 fractions originating from reforming and from steam cracking, respectively (1–11). The demand for paraxylene, already very significant, is continuously increasing: approximately 8% per year during the past 10 years (9); paraxylene is oxidized to terephthalic acid which is used in the production of polyester films and fibers. Separation of ethylbenzene that is used for the production of styrene requires high efficiency, and hence expansive distillation. It is why, in the commercial units, ethylbenzene separation is generally omitted.

To meet the demand for paraxylene, the much less used meta- and orthoxylenes have to be converted to additional paraxylene. This isomerization being limited by thermodynamic equilibrium, the separation process plays a significant role in paraxylene production. Separation of paraxylene was first carried out by crystallization. However, the high cost of equipment, high energy consumption, and limited yield of crystallization have led to the substitution of selective adsorption on molecular sieves for crystallization (5, 12). The raffinate going out of the separation unit enters the isomerization unit in which the thermodynamic equilibrium between xylene isomers is reestablished. In the isomerization unit, ethylbenzene must be transformed in order to avoid its build-up in the recycle stream, with a minimum loss and even if possible a gain in xylenes.

The isomerization processes differ in the way ethylbenzene is converted, either by isomerization into xylenes or by dealkylation or transalkylation into products which can be easily separated (1, 3, 5–9). In the first type of process which has the advantage of increasing xylene production, bifunctional catalysts containing an acidic mordenite in

[1] To whom correspondence should be addressed. Fax: +33-(0)5-49-45-37-79. E-mail: michel.guisnet@univ-poitiers.fr.

0021-9517/01 $35.00

combination with platinum supported on alumina are generally used (5–9). Indeed, whereas xylene isomerization can occur through acid catalysis, ethylbenzene isomerization can proceed only through bifunctional catalysis. In the literature, there is a good agreement with the following mechanism for ethylbenzene isomerization: hydrogenation of ethylbenzene (EB) into traces of ethylcyclohexenes (ECHE), acid isomerization of the very reactive ethylcyclohexenes into dimethylcyclohexenes (DMCHE), and then dehydrogenation of dimethylcyclohexenes into xylenes (X) (3, 13–16):

$$\text{EB} \rightleftharpoons \text{ECHE} \rightleftharpoons \text{DMCHE} \rightleftharpoons \text{X}.$$

Under the conditions used for isomerization, ethylbenzene (and xylenes) can undergo various secondary reactions (3, 4, 6–9, 14, 17): hydrogenation into saturated naphthenes over the metallic sites, disproportionation, transalkylation and dealkylation over the acidic sites, and isomerization and hydrocracking of naphthenes through bifunctional catalysis. Mordenite was generally chosen as the acid component because in the narrow channels of this zeolite disproportionation and transalkylation are limited by steric constraints (3). Furthermore, modifications of the acidity and porosity of the mordenite component (e.g., by dealumination) are expected to lead to a significant improvement in the selectivity to isomers.

This paper compares the results obtained in a large range of contact times for ethylbenzene transformation over a series of intimate mixtures of 0.5 wt% Pt/Al_2O_3 (75 wt%) and of mordenites (25 wt%) with Si/Al ratios between 6.6 and 180, hence with large differences in acidity and porosity. The aim is to understand the effect of these acidity and porosity characteristics on the rates of ethylbenzene isomerization and of the secondary reactions as well as on the selectivity to xylene products.

EXPERIMENTAL PART

1. *Catalysts*

Mordenite samples will be called HMOR followed by the approximate value of the total Si/Al: HMOR6.6 was supplied by the "Institut Régional des Matériaux Avancés" (IRMA) in Ploemeur, France. HMOR10 was a commercial product from TOSOH, Amsterdam, The Netherlands. HMOR20 was provided by PQ Zeolites B. V., Amsterdam, The Netherlands. The other mordenite samples with Si/Al equal to 30, 45, 90, 120, and 180 were prepared by dealumination of HMOR20 by HNO_3 solutions at reflux for 4 h in one or two steps with HNO_3 normalities ranging from 6 to 14.5. The volume of HNO_3 solution/catalyst weight ratio was equal to 10. Chemical compositions of all the mordenite samples are grouped in Table 1.

Sorption isotherms for nitrogen at 77 K over HMOR samples were recorded using a gas adsorption system ASAP 2010 (Micromeritics), the samples being previously pretreated at 653 K for 2 h under secondary vacuum.

The acidity of HMOR samples was characterized by pyridine adsorption followed by IR spectroscopy using a Nicolet MAGNA IR 550 spectrometer. Thin wafers of about 8 mg cm^{-2} were pretreated *in situ* in the IR cell under air flow: 60 ml min^{-1} at 773 K for 12 h and then in a vacuum (10^{-3} Pa) at 673 K for 1 h. Pyridine was adsorbed on the samples at 423 K. The IR spectra were recorded at room temperature after the activation period and after pyridine thermodesorption in vacuum (10^{-3} Pa) at various temperatures: 423, 523, 623, and 723 K.

Pt/Al_2O_3 (PtA) was prepared by ion exchange of γ-Al_2O_3 with a hexachloroplatinic acid solution followed by calcination at 773 K under dry air for 4 h. The Pt content was equal to 0.53 wt%. The Pt dispersion determined by H_2–O_2 titration after reduction under hydrogen flow (30 ml min^{-1}) at 693 K for 12 h was close to 100%.

The bifunctional Pt/Al_2O_3 + H-mordenite catalysts were prepared by milling the mixture of the two components (75 wt% Pt/Al_2O_3 + 25 wt% H-mordenite) and then pelletizing and sieving at 0.2–0.4 mm.

2. *Ethylbenzene Transformation*

The transformation of ethylbenzene (Fluka puriss product percolated on silica gel before use) was carried out in a fixed-bed stainless steel reactor under the following conditions: temperature = 683 K, total pressure = 10 bar, H_2/ethylbenzene molar ratio = 4, WHSV (weight hourly space velocity) = 5–200 g of ethylbenzene h^{-1} g^{-1} of catalyst. Before use, the catalysts were treated *in situ* under H_2 (10 bar, 600 ml min^{-1} g^{-1}) at 753 K for 4 h. Reaction products were analyzed on-line by FID gas chromatography (GC) using two fused silica J&W capillary columns: a 30-m DB-Wax and a 60-m DB-1, the first one for the separation of ethylbenzene and xylene isomers and the second one to obtain the distribution of all the products. Preliminary experiments have shown that a constant surface area of the GC peaks was obtained for a time on stream (TOS) of 30–40 min. Therefore, with all the catalysts, the first analysis of the reaction products was carried out at TOS = 45 min.

RESULTS AND DISCUSSION

1. *Characteristics of the Zeolite Samples*

The unit cell formula of all the samples (Table 1) was determined from elemental analysis and from the values of framework Si/Al ratio estimated from ^{29}Si NMR or from the position of the IR structure bands. With most of the samples (except HMOR10 and HMOR20), the number of extraframework aluminum species (EFAL) per unit cell

TABLE 1

Characteristics of the Mordenite Samples[a]

Sample	Unit cell formula	EFAL	Pore volume ($cm^3 \cdot g^{-1}$)		Acidity		
			Micro	Meso	N_{H^+}	N_L	N_{H^+}/N_{th}
HMOR6.6	$Na_{0.14}H_{6.16}Al_{6.30}Si_{41.70}O_{96}$	0	0.14	0.01	3.20	0	0.52
HMOR10	$Na_{0.01}H_{3.68}Al_{3.69}Si_{44.31}O_{96}$	0.35	0.19	0.04	2.54	0.18	0.69
HMOR20	$Na_{0.05}H_{1.95}Al_2Si_{46}O_{96}$	0.20	0.18	0.11	1.19	0.31	0.61
HMOR30	$Na_{0.006}H_{1.344}Al_{1.35}Si_{46.65}O_{96}$	0.05	0.18	0.13	0.63	0.15	0.47
HMOR45	$Na_{0.004}H_{0.996}Al_1Si_{47}O_{96}$	0	0.18	0.13	0.44	0.04	0.44
HMOR90	$Na_{0.003}H_{0.507}Al_{0.51}Si_{47.49}O_{96}$	0	0.14	0.13	0.28	0.06	0.56
HMOR120	$Na_0H_{0.35}Al_{0.35}Si_{47.65}O_{96}$	0	0.15	0.13	0.23	0.07	0.66
HMOR180	$Na_0H_{0.21}Al_{0.21}Si_{47.79}O_{96}$	0	0.14	0.14	0.15	0.075	0.71

[a] EFAL: extraframework aluminum species. N_{th}: number of protonic sites per unit cell estimated from the unit cell formula. N_{H^+}, N_L: number of protonic sites (H^+) and of Lewis (L) sites per unit cell able to retain pyridine adsorbed at 423 K.

is negligible in comparison to the number of framework aluminum species. Furthermore, with all the samples the number of sodium atoms per unit cell is very low (Table 1).

With HMOR6.6 and −10, a type I isotherm was obtained from nitrogen adsorption, which indicates that these zeolites contain essentially micropores. With all the other zeolites, the shape of the isotherms was different, showing the presence of mesopores in addition to micropores. In the series of samples resulting from HMOR20, dealumination causes a decrease in the micropore volume and a small increase in the mesopore volume.

The following OH bands can be observed in the IR spectra of mordenite samples: at 3744 cm^{-1} corresponding to silanol groups in silicon-rich debris, at 3736 cm^{-1} to silanols due to framework defects, at 3660 cm^{-1} to OH linked to extraframework Al species, and at 3610 cm^{-1} corresponding to bridged OH groups (18). Dealumination of HMOR20 causes an increase of the silanol bands, the decrease of the 3610 cm^{-1} band, and the disappearance of the 3660 cm^{-1} band (Figs. 1B, 1C, 1D). With HMOR6.6 and −10 (Fig. 1A), pyridine adsorption results only in a decrease of the 3610 cm^{-1} band, whereas with the other samples, this band disappears completely (Figs. 1B, 1C, 1D). This indicates that all the hydroxyls located in the side pockets of the latter samples interact with pyridine molecules, which is not the case for those of HMOR6.6 and −10. As was previously proposed with another series of mordenite samples (19), this change in the effect of pyridine would be mainly due to an increase with dealumination in the accessibility of the protonic sites located in the side pockets. Figure 1 shows also that part of the silanol groups and of the extraframework aluminum species interact with pyridine. The interaction of the silanol groups results in the shift of the corresponding band to lower frequency values as clearly shown with the more dealuminated samples, e.g., appearance of a new band at 3680–3700 cm^{-1} after pyridine adsorption over HMOR120 (curve b), and hence of a negative band in curve c corresponding to acidic hydroxyls (Figs. 1C, 1D). Another large band also appears at 3420–3480 cm^{-1}, which could be related to hydrogen bonding between pyridine molecules and bridged hydroxyls located in the side pockets with a shift to lower frequency values of the corresponding band.

The concentrations of Brønsted and Lewis sites were estimated from the intensities of the bands at 1545 cm^{-1} (PyH^+) and 1450 cm^{-1} (PyL) by using the values of extinction coefficients measured in a previous study (19). Table 1 shows that N_{H^+}, the number of protonic sites per unit cell able to retain pyridine at 423 K as pyridinium ions is always lower (1.4 to 2 times) than the theoretical number given in the unit cell formula N_{th} (e.g., for HMOR6.6, $N_{th} = 6.16$ and $N_{H^+} = 3.2$, Table 1). This could be explained by the

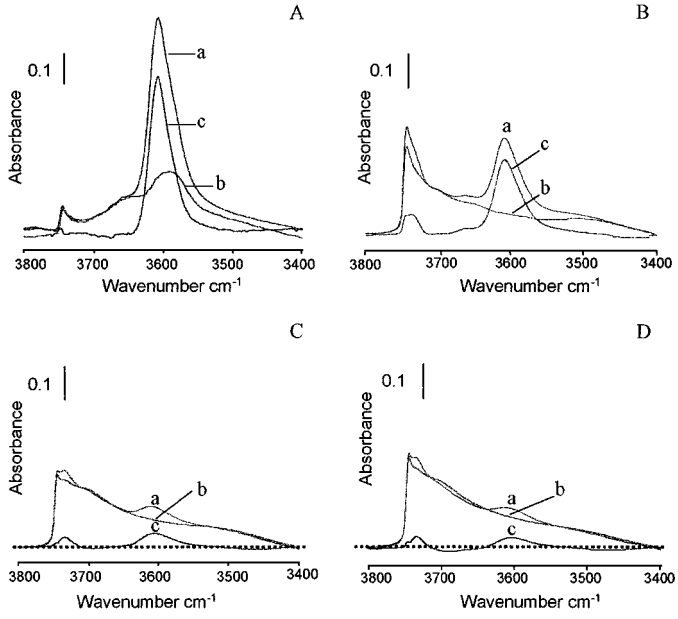

FIG. 1. IR spectra of OH groups in HMOR10 (A), HMOR20 (B), HMOR 90 (C), and HMOR120 (D). Spectra: (a) activated mordenites, (b) after pyridine adsorption at 423 K, (c) difference of spectra a–b.

impossibility for pyridine molecules to interact with protonic sites of the narrow channels (HMOR6.6 and HMOR10) or to be adsorbed as pyridinium ions (other HMOR samples). Whatever the sample, the number of Lewis sites per unit cell able to retain pyridine adsorbed at 423 K (N_L) is much lower than N_{H^+} (Table 1).

It should be noticed that part of the protonic sites of HMOR6.6, −10, and −20 are able to retain pyridine adsorbed at 723 K, suggesting the existence of very strong sites. Furthermore, the ratio between the number of protonic sites able to retain pyridine adsorbed at 623 K and at 423 K is equal to 0.3–0.35 with HMOR6.6, 10, 20, and 30, and then decreases when the Si/Al ratio increases: 0.16, 0.12, and 0.08 for Si/Al 90, 120, 180 respectively, which suggests a decrease in acid strength.

2. *Activity, Stability of the Catalysts, and Product Distribution*

With all the catalysts, ethylbenzene transformation was first carried out for approximately 12–15 h at a weight hourly space velocity (WHSV) of 15 h^{-1}, and then at different WHSV values (hence different contact times) for 1 to 6 h, and then finally at WHSV of 15 h^{-1}. Figure 2 shows that there is during the first period a decrease in conversion due to coke formation (20) followed by a plateau: the values of conversion before and after experiments at different contact times (i.e., at 15 and 40 h of reaction) are very close. Dealumination leads to a slight increase in stability. Thus, the ratios of activity between 12 h and 45 min pass from 0.70 with HMOR20 to 0.83 with HMOR180. It should be remarked that the stability of purely acidic catalysts, e.g., mixture 75 wt% Al_2O_3 and 25 wt% HMOR10 or HMOR90 (A-HMOR10 and A-HMOR90), is similar to the stability of the corresponding bifunctional catalysts.

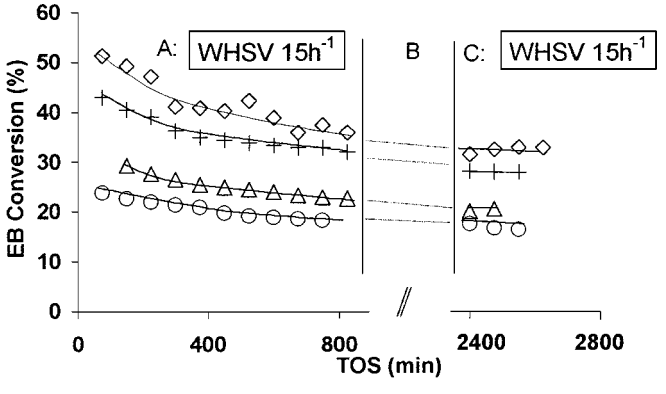

FIG. 2. Conversion of ethylbenzene versus time on stream (TOS) at various contact times. (A) Conversion on fresh catalysts (PtA-HMOR10 (+), PtA-HMOR20 (◇), PtA-HMOR90 (Δ), and PtA-HMOR120 (○)) at a weight hourly space velocity (WHSV) of 15 h^{-1}. (B) Experiments at different space velocities (hence different contact times); WHSV equal to 5, 30, 60, and 150 h^{-1}. (C) Conversion at WHSV of 15 h^{-1}.

TABLE 2

Activity (10^{-3} mol h^{-1} g^{-1} Catalyst) of the Acid (A-HMOR) and of the Bifunctional (PtA-HMOR) Catalysts in Ethylbenzene Transformation (Total), and in Isomerization (Isom), Disproportionation (Disp), Dealkylation (Dealk), and Production of C_8 Naphthenes (Hydrog) and of Ethylcyclohexane (ECH, in Parentheses)

	Activity				
Catalyst[a]	Total	Isom	Disp	Dealk	Hydrog (ECH)
PtA-HMOR6.6	47.3	8.1	19.6	1.8	17.8 (9)
PtA-HMOR10	111.5	14.5	69.5	5.7	21.8 (7.5)
PtA-HMOR20	151	7.3	115	13.3	15.4 (6.2)
PtA-HMOR30	60.9	11.1	28.6	3.1	18.1 (7.7)
PtA-HMOR45	61.0	11.4	24.2	2.6	22.8 (7.6)
PtA-HMOR90	50.2	13.6	10.4	1.2	25.0 (17.6)
PtA-HMOR120	39.7	9.9	7.1	1.0	21.7 (12.5)
PtA-HMOR180	25	4.0	1.6	0.6	18.8 (15.6)
A-HMOR10	114.2	0	103	11.2	0
A-HMOR90	13.6	0	12.4	1.2	0
A-PtA	14.4	0	0	0	14.4 (14.4)

[a] PtA: 0.53 wt% Pt/γ-Al_2O_3. A: γ-Al_2O_3.

Furthermore, the Pt-Al_2O_3 component of the bifunctional catalysts, actually the Al_2O_3 (25 wt%)–Pt-Al_2O_3 (75 wt%) mixture (A-PtA), is only active for ethylbenzene hydrogenation (last line, Table 2) and its stability is quasi perfect.

For each catalyst, the conversion of ethylbenzene at the plateau was plotted as a function of contact time τ (taken here as the reverse of WHSV) and the activity estimated from the slope of the initial tangents to the curves (Fig. 3). PtA-HMOR20 and PtA-HMOR10 are the most active catalysts, the more dealuminated sample (PtA-HMOR180) being the least active (Table 2).

The distribution of reaction products obtained (on the stabilized catalysts) for a conversion of 35% over the PtA-HMOR samples and over A-HMOR10 is reported in

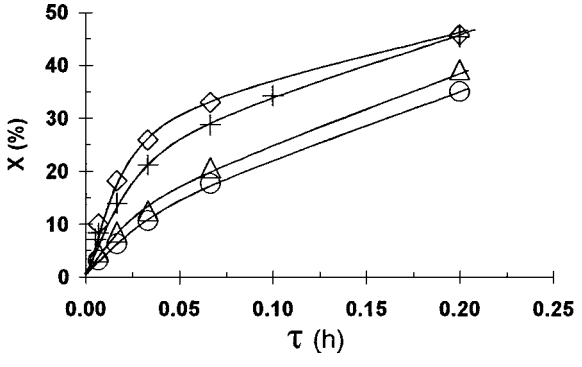

FIG. 3. Ethylbenzene transformation on PtA-HMOR10 (+), PtA-HMOR20 (◇), PtA-HMOR90 (Δ), and PtA-HMOR120 (○). Conversion (X, %) versus contact time τ (h) (τ is taken as the reverse of the weight hourly space velocity, WHSV).

TABLE 3

Distribution (Wt%) of All the Products of Ethylbenzene Transformation[a]

	PtA-HMOR6.6	PtA-HMOR10	PtA-HMOR20	PtA-HMOR90	PtA-HMOR120	A-HMOR10
Conversion	34.2	34.2	34.9	37.6	35	37.9
C_2	1.9	3.2	6	1.5	1.3	8.5
C_3	1.3	1.7	1.8	1.1	1.1	1.4
C_4 (i/n)	2.2 (1.6)	3.0 (1.5)	2.5 (1.39)	2.0 (1.27)	2.0 (1.21)	1.2 (1.61)
C_5 (i/n)	0.9 (2.57)	1.3 (1.84)	1.0 (2.03)	1.0 (1.78)	1.1 (1.72)	0.4 (4.33)
C_6	0.6	0.8	0.8	0.5	0.5	0.3
N_6	3.4	3.9	2.7	2.5	2.1	0.7
N_7	0.4	0.5	0.2	0.2	0.2	0.2
N_8	14.8	10.8	5.6	10.9	13.2	0.8
Benzene	14.3	22.2	36.3	10.1	8.7	50.3
Toluene	2.9	3.1	2.2	2.8	2.5	1.9
Xylenes	37.3	24.1	6.6	47.8	53.9	0.4
ET	2.8	3.1	2.6	2.7	2.1	2.4
TMB	0.3	0.2	0	0.4	0.3	0
DEB	14.4	19.6	28.8	12.5	9	29.2
DMEB	1.0	0.8	0.4	1.8	1.2	0.3
C_{10+}	1.5	1.7	2.5	2.2	0.8	2.0
	100	100	100	100	100	100

[a] N_6, N_7, N_8: C_6, C_7, C_8 naphthene. ET: ethyltoluenes. TMB: trimethylbenzenes. DEB: diethylbenzenes. DMEB: dimethylethylbenzenes.

Table 3. With the bifunctional catalysts, the following products were observed:

- C_2–C_6 alkanes.
- C_6–C_8 naphthenes, cyclohexane and methylcyclopentane (N_6); methylcyclohexane and dimethylcyclopentanes (N_7); ethylcyclohexane and isomers, dimethylcyclohexanes, ethylmethylcyclopentanes, and trimethylcyclopentanes (N_8).
- C_6–C_{10+} aromatic hydrocarbons: benzene, toluene, xylenes (X), ethyltoluenes (ET), trimethylbenzenes (TMB), diethylbenzenes (DEB), dimethylethylbenzenes (DMEB), and C_{11+} (formed only at very high conversions).

These products result from six main transformations of ethylbenzene or/and of the primary products:

1. Isomerization of ethylbenzene into ortho-, meta- and paraxylenes.
2. Disproportionation of ethylbenzene into benzene and diethylbenzenes.
3. Dealkylation of ethylbenzene into benzene and ethylene totally transformed into ethane (or into longer alkanes).
4. Transalkylation of ethylbenzene–xylenes which leads to ethyltoluene (ET) and toluene or to dimethylethylbenzene (DMEB) and benzene.
5. Hydrogenation of C_8 aromatics (with isomerization of the products).
6. Cracking of C_8 naphthenes (N_8) into C_3–C_6 alkanes.

It should be remarked that additional reactions are necessary to explain the formation of N_6, N_7 naphthenes (probably hydrogenation of benzene and toluene and then isomerization), of trimethylbenzenes (disproportionation of xylenes), and of heavy aromatic products. Furthermore, part of the C_3–C_6 alkanes could result from transformation of ethylene through oligomerization–cracking steps followed by hydrogenation. However, with the bifunctional catalysts, there is a good agreement between the experimental values of the yields in benzene and the corresponding values calculated from the yields in DEB, DMEB, and ethane (produced simultaneously with benzene), which indicates that the oligomerization–cracking process can be neglected.

With the purely acid catalysts, reactions 1, 5, and 6 do not occur at low conversions and are practically negligible at high conversions. C_3–C_6 hydrocarbons which are observed do not result from naphthene cracking but from oligomerization–cracking of ethylene resulting from dealkylation: indeed, the experimental values of the benzene yield are equal to the calculated values, only if it is considered that C_3–C_6 hydrocarbons result from ethylene transformation.

With Pt-Al_2O_3 (actually A-PtA), ethylcyclohexane is the only product at low conversions. At high conversions, trimethyl- and ethylmethylcyclopentanes appear in low amounts resulting from ethylcyclohexane transformation.

From the comparison of A-PtA, PtA-HMOR, and A-HMOR, it can be concluded that reactions 2–4 occur through acid catalysis, hydrogenation through metal catalysis, the second part of reaction 5 (isomerization of N_8), reaction 1 (isomerization), and reaction 6 (cracking) through bifunctional catalysis (21).

For each catalyst, the conversion of ethylbenzene through the six main reactions presented above was plotted as a function of contact time (1/WHSV from to 0.005 to 0.2 h). and as a function of total conversion. With the bifunctional catalysts, the slope of the tangent to the curves at zero conversion was positive for reactions 1, 2, 3, and 5 (the corresponding products are primary) and equal to zero for the products of reactions 4 and 6 which are therefore secondary products (Fig. 4). The secondary nature of these latter products was quite expected since ethylbenzene–xylenes transalkylation is necessarily consecutive to isomerization, and cracking is consecutive to naphthene formation. Another important remark is that whereas the conversion of ethylbenzene through isomerization, dealkylation, transalkylation, and cracking increases continuously with contact time, this is not the case for the conversion into disproportionation products which passes through a maximum with the most active catalysts (i.e., at high conversions) and especially for the conversion into C_8 naphthenes.

For the formation of these C_8 naphthenes (Fig. 5), a quasi plateau in conversion is obtained from short contact times: 1/WHSV equal to 0.03 h. The plateau is obtained even at shorter contact times when only ethylcyclohexane is considered (Fig. 6). This suggests that thermodynamic equilibrium between ethylbenzene and ethylcyclohexane and even the isomers of ethylcyclohexane is rapidly established. The conversion at thermodynamic equilibrium of ethylbenzene into ethylcyclohexane was estimated to be equal to 2% from the values of the standard Gibbs energies of formation (22). Values very close to this thermodynamic value were obtained on pure PtA for contact times greater than 0.03 h. With the bifunctional catalysts, the maximum percentage of ethylcyclohexane was lower (Fig. 6). This lower value seems to be due to a rapid isomerization of ethylcyclohexane. Indeed, the more significant this isomerization, the lower the maximum percentage of ethylcyclohexane.

The distribution of xylenes depends on contact time, and hence on ethylbenzene conversion, as shown in Fig. 7. At

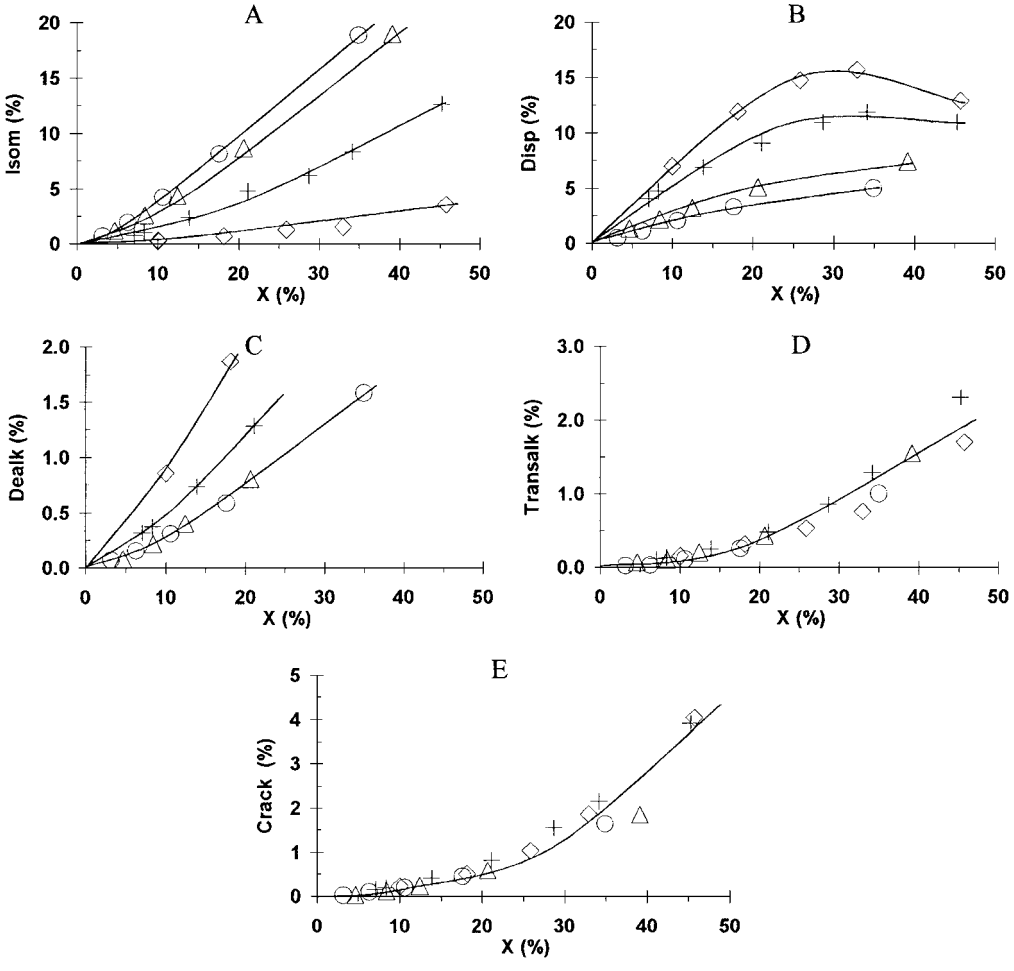

FIG. 4. Ethylbenzene transformation on PtA-HMOR10 (+), PtA-HMOR20 (◇), PtA-HMOR90 (Δ), and PtA-HMOR120 (○). (A) Yield in isomers (Isom), (B) yield in disproportionation products (Disp), (C) yield in dealkylation products (Dealk), (D) yield in transalkylation products (Transalk), and (E) yield in cracking products (crack) versus conversion of ethylbenzene (X, %).

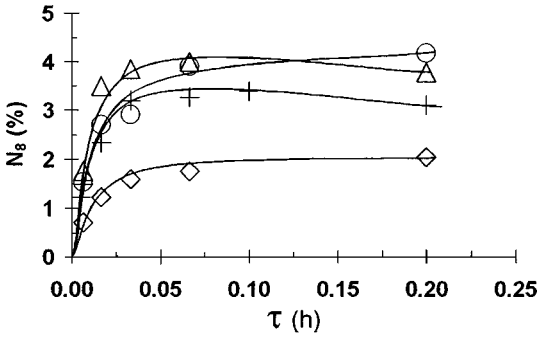

FIG. 5. Ethylbenzene transformation on PtA-HMOR10 (+), PtA-HMOR20 (◇), PtA-HMOR90 (Δ), and PtA-HMOR120 (○). Yield in C_8 naphthenes (N_8) versus contact time τ (h) (τ is taken as the reverse of the weight hourly space velocity, WHSV).

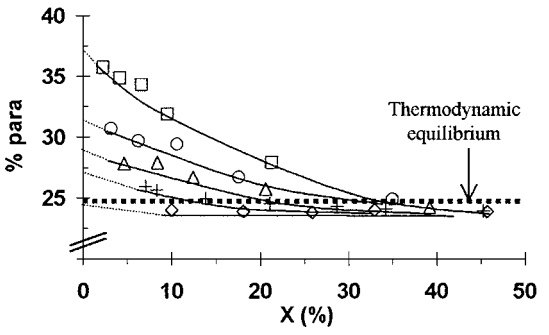

FIG. 7. Change in the percentage of *p*-xylene (% para) in the xylene mixture as a function of ethylbenzene conversion (X, %): PtA-HMOR10 (+), PtA-HMOR20 (◇), PtA-HMOR90 (Δ), PtA-HMOR120 (○), and PtA-HMOR180 (□).

low conversion, the proportion of paraxylene is greater than that at thermodynamic equilibrium (25.1% (22)), whereas the proportion of metaxylene is lower. The difference between experimental and equilibrium values increases with the degree of dealumination (Fig. 7). For conversions greater than 10–20%, the xylene distribution is very close to the thermodynamic equilibrium distribution (Fig. 7). Disproportionation of ethylbenzene leads also at low conversion to a mixture of diethylbenzenes (DEB) richer in para isomer than at equilibrium: e.g., 36.2% para, 58.2% meta, 5.6% ortho with PtA-HMOR6.6 and 68% para, 31% meta, and 1% ortho with PtA-HMOR180 at zero conversion instead of 28% para, 52% meta, and 20% ortho at thermodynamic equilibrium (22, 23). The preferential formation of para isomers suggests the existence of shape selectivity effects. However, this proposal is in contradiction with the increase in selectivity to para isomers with the degree of dealumination, and hence with the accessibility to the acid sites. A tentative suggestion is that this increase is due to the significant decrease in disproportionation (Fig. 4); indeed disproportionation of para isomers on a HFAU zeolite was shown to be faster than disproportionation of meta and ortho isomers (24).

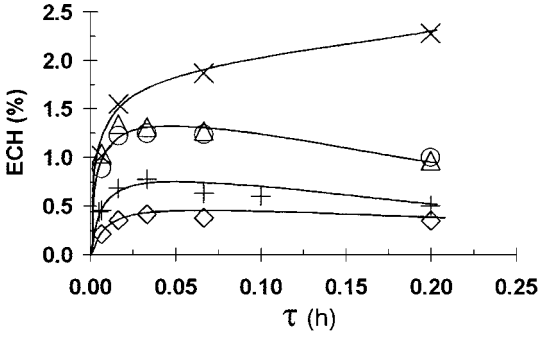

FIG. 6. Ethylbenzene transformation on A-PtA (×), PtA-HMOR10 (+), PtA-HMOR20 (◇), PtA-HMOR90 (Δ), and PtA-HMOR120(○). Yield in ethylcyclohexane (ECH) versus contact time τ (h) (τ is taken as the reverse of the weight hourly space velocity, WHSV).

3. Influence of the Catalyst Characteristics on the Initial Rates

It should be remarked that all the catalytic results discussed here were obtained at the plateau of conversion, whereas the physicochemical characteristics were established on the fresh catalysts. However, the degree of desactivation depends only slightly on the catalyst: the ratio between ethylbenzene conversion at 12 h and 45 min is between 0.70 and 0.83 with all the bifunctional catalysts. Moreover, there is practically no difference between the product distributions measured at isoconversion on the fresh and the stabilized catalysts. Therefore, the correlations between rates and physicochemical properties which are presented hereafter can be considered as semiquantitatively valid.

The initial rates of reactions 1, 2, 3, and 5 were estimated from the values of the slopes at zero conversion of the tangents to the curves of yields versus contact time. It should be remarked that there is a large imprecision in the values of hydrogenation rates because of the rapid establishment of a plateau in conversion corresponding to thermodynamic equilibrium. However, as can be expected, similar values are found for the rates of formation of C_8 naphthenes with all the bifunctional catalysts and with A-PtA (Table 2). Moreover, the rates of ethylcyclohexane formation are similar on A-PtA and on the bifunctional catalysts with highly dealuminated HMOR as the acid component for which the isomerization of ethylcyclohexane is relatively slow.

Table 2 shows that with all the bifunctional catalysts, hydrogenation is the fastest reaction. Disproportionation is also very fast whereas dealkylation is very slow. Finally, the initial rate of isomerization depends very much on the catalyst. To discuss the effect of the protonic sites on the rates of reactions 1, 2, and 3 which occur through acid or bifunctional catalysis, the turnover frequency values (TOF) were estimated by dividing the initial rates by n_{H^+} the concentration of protonic sites per gram of catalyst drawn from pyridine adsorption experiments.

For the acidic reactions 2 and 3, the TOF values were plotted versus n_{H^+} (Figs. 8A, 8B). Figure 8A shows that with the series of dealuminated samples (Si/Al from 20 to 180), TOF for disproportionation is proportional to n_{H^+}, and hence that the catalyst activity is proportional to $(n_{H^+})^2$. This relation is the one expected for reactions requiring two protonic sites for their catalysis (25, 26), which would be the case for disproportionation occurring through diphenylmethane intermediates (21, 27) (Fig. 9): two different protonic sites would be involved in steps 1–3 and steps 4–6. With large-pore zeolites, this mechanism is more likely than the deethylation–ethylation mechanism which was shown to occur with average pore size zeolites (28, 29). Therefore, the density of acid sites seems to be the parameter determining the disproportionation rate, the acidic strength (higher with HMOR20 than with the other zeolites) having apparently no effect. However, the relationship between TOF and n_{H^+} is not valid for PtA-HMOR6.6 and −10 and A-HMOR10. The very low values of the TOF found with these catalysts are probably related to the quasi absence of mesopores in these zeolites (Table 1). Indeed, it is well demonstrated that mesopores play a significant role in reactions catalyzed by monodimensional zeolites allowing a quasi tridimensional diffusion of organic molecules (30, 31). In the absence of mesopores, reactant transformation would be significantly limited by diffusion, and hence would occur only in the outer part of the crystallites. Only a small part of the protonic sites would therefore participate in reactions with therefore very low reaction rates and TOF values.

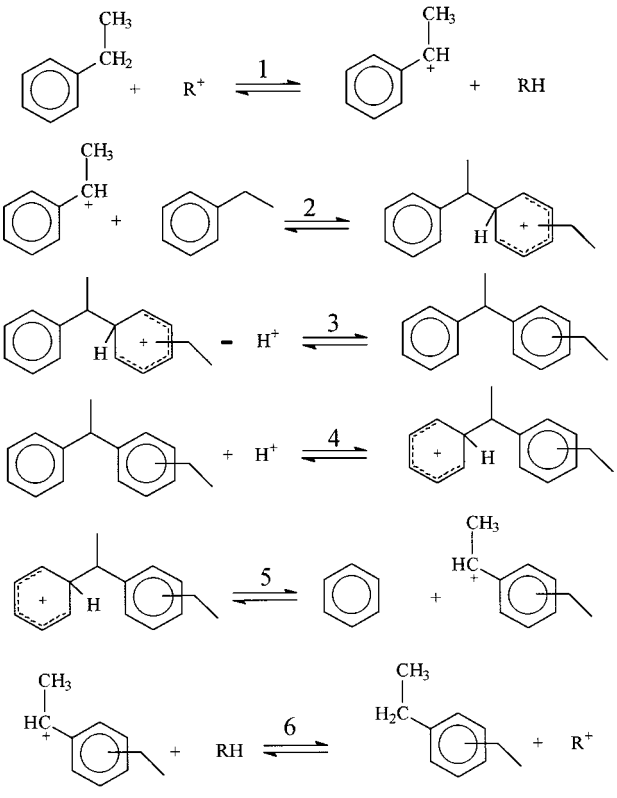

FIG. 9. Mechanism of ethylbenzene disproportionation over large-pore zeolites.

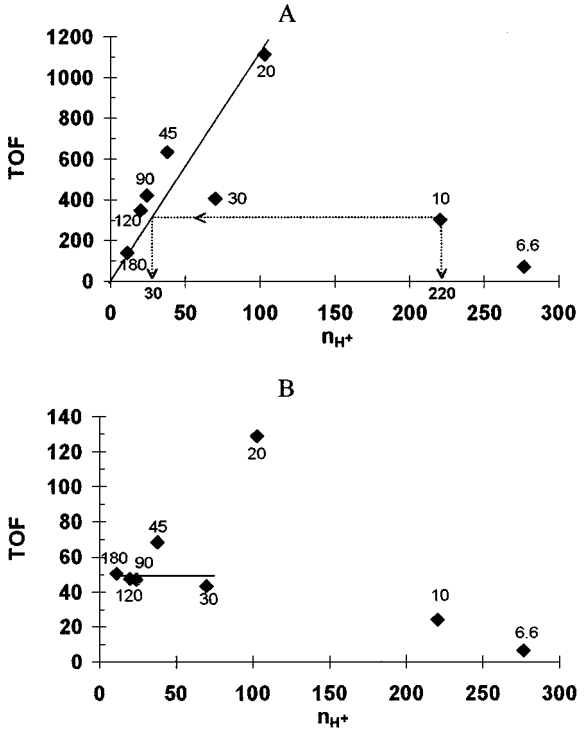

FIG. 8. Turnover frequency values TOF (h^{-1}) for disproportionation (A) and for dealkylation (B) versus the concentration of protonic sites per gram of catalyst, n_{H^+} (μmol g^{-1} catalyst) able to retain pyridine adsorbed at 423 K.

This part (actually the effectiveness factor η of the catalyst) can be roughly estimated from the linear correlation between TOF and n_{H^+}. Thus, with PtA-HMOR10, the n_{H^+} value corresponding to the experimental value of TOF (310 h^{-1}) is equal to 30 μmol g^{-1} of catalyst (Fig. 8A) instead of the measured value of 220, which means that only 14% of the protonic sites of HMOR10 would participate in disproportionation ($\eta = 0.14$). With PtA-HMOR6.6, the percentage of the active protonic sites estimated by the same way is equal to less than 3% ($\eta = 0.03$).

The TOF values obtained for dealkylation with PtA-HMOR6.6, PtA-HMOR10, and A-HMOR10 are also lower than for the other samples (Fig. 8B). Furthermore, quasi identical values of TOF are found with the other samples, except with PtA-HMOR20 which is 2.5 times more active. This could be ascribed to the presence of very strong acidic sites on HMOR20, able to retain pyridine adsorbed at 723 K. For this monomolecular reaction which therefore requires only one acid site for its catalysis, there is as expected no effect of the density of the acidic sites. It should be remarked that TOF in dealkylation is lower (3–10 times depending

on the sample) than TOF in disproportionation. Therefore, it is most likely that dealkylation requires stronger acid sites than disproportionation. This could be foreseen from the reaction mechanism, disproportionation requiring the following carbocations which present a high stability,

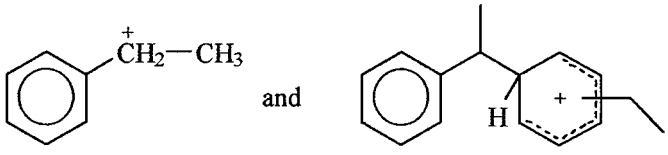

whereas dealkylation requires the formation of a very unstable ethyl carbenium ion CH_3–CH_2^+. The high acid strength required for dealkylation could explain why the presence of very strong acid sites (e.g., on HMOR20) has a very positive effect on the TOF in dealkylation. For disproportionation which does not require a high acidic strength, the effect of this parameter on TOF should be more limited, and hence would be masked by the large effect of the acid site density.

The part of the protonic sites of HMOR6.6 and HMOR10 which participate in dealkylation (actually the effectiveness factor η) can be estimated from the comparison between their TOF values and those of the other catalysts. As the strength of the protonic sites of HMOR6.6 and HMOR10 is comparable to that of HMOR20, the TOF value of this latter catalyst was chosen to estimate η. Only 5% of the protonic sites of HMOR6.6 ($\eta = 0.05$) would participate in ethylbenzene dealkylation, which would be the case for 19% of the sites of HMOR10.

As is expected for reactions occurring through bifunctional catalysis (32–36), the balance between hydrogenating and acid functions determines for a large part the catalyst activity and the TOF of the protonic sites for ethylbenzene isomerization. Figure 10 shows the change of TOF versus n_{Pt}/n_{H^+}, the ratio between the concentrations of accessible platinum atoms and of protonic sites able to retain pyridine adsorbed at 423 K, taken as representative of the hydrogenating/acid function balance. The shape of the curve is the one expected from a bifunctional catalysis: at low value of n_{Pt}/n_{H^+}, TOF increases with this ratio, which means that the limiting step is catalyzed by the metallic sites whereas at high values, TOF is constant, i.e., the limiting step is catalyzed by the acidic sites. Curiously, the values obtained with PtA-HMOR6.6 and −10 seem to be located on the curve. This can be explained by a compensation effect: indeed, in the crystallites of these mordenite samples which do not present mesopores, the transformation of the olefinic intermediates is, like ethylbenzene disproportionation or dealkylation, significantly limited by diffusion, and hence would occur only in the outer part of the crystallites. Thus, the ratio between the concentrations of accessible Pt atoms and of *accessible* protonic sites is greater than the calculated n_{Pt}/n_{H^+} value. On the other hand, the actual TOF value (i.e., per *accessible* protonic site) is greater than the value reported in Fig. 10.

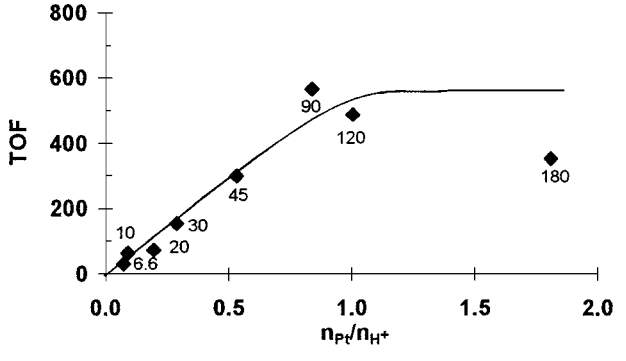

FIG. 10. Turnover frequency values TOF (h^{-1}) for ethylbenzene isomerization versus the ratio between the number of accessible platinum atoms (n_{Pt}) and the concentration of protonic sites (n_{H^+}) able to retain pyridine adsorbed at 423 K.

Similar curves are also obtained for the formation of dimethylcyclohexanes, methylethylcyclopentanes, and trimethylcyclopentanes which result from ethylcyclohexane isomerization through bifunctional catalysis.

4. *Influence of the Zeolite on the Product Distribution*

The distributions of the products obtained over the bifunctional catalysts were compared at various conversions. Practically no difference was observed between the distributions on the fresh and on the stabilized catalysts, provided however that these distributions are compared at isoconversion. The distributions (per reaction) determined for zero (extrapolated values) and for 35% conversion are given in Table 4. A large effect of conversion can be observed: a significant increase in the percentages of isomerization and dealkylation, the appearance of cracking and transalkylation products at high conversions, and a significant decrease in disproportionation and hydrogenation. All of these changes could be expected from the shape of the curves giving conversions versus contact time. The decrease in disproportionation is due to the establishment of thermodynamic equilibrium and to the secondary transformation of diethylbenzenes (shown by a maximum in Fig. 4B) by dealkylation into ethylene which is rapidly hydrogenated and into ethylbenzene which can undergo other transformations. The plateau in hydrogenation products (Fig. 5) is due to the establishment of thermodynamic equilibrium for low values of contact time and hence a low value of conversion. Cracking products result from secondary transformation of C_8 naphthenes, and transalkylation products from secondary transformation of xylenes with ethylbenzene. This secondary transformation of xylenes is slow compared to their rate of formation and the percentage of xylenes increases significantly at the expense of those of hydrogenation and of disproportionation.

TABLE 4

Distribution (Wt%) of the Reaction Products Extrapolated at Zero Conversion (A) and at 35% Conversion of Ethylbenzene (B) in Isomerization (Isom), Disproportionation (Disp), Dealkylation (Dealk), Cracking Products (Crack), and Production of C_8 Naphthenes (Hydrog)[a]

Catalyst	Isom	Disp	Dealk	Crack	Hydrog	Transalk
			A			
PtA-HMOR6.6	17.1 (27.4)	41.4	3.8	0	37.6	0
PtA-HMOR10	13.0 (16.2)	62.3	5.1	0	19.6	0
PtA-HMOR20	4.8 (5.3)	76.2	8.8	0	10.2	0
PtA-HMOR30	18.2 (25.9)	47.0	5.1	0	29.7	0
PtA-HMOR45	18.7 (29.9)	39.6	4.3	0	37.4	0
PtA-HMOR90	27.1 (54.0)	20.7	2.4	0	49.8	0
PtA-HMOR120	24.9 (55.0)	17.9	2.5	0	54.7	0
			B			
PtA-HMOR6.6	41.4 (46.3)	29.7	8.3	5.8	10.6	4.2
PtA-HMOR10	28.4 (31.6)	37.1	12.5	7.1	10.2	4.4
PtA-HMOR20	6.9 (7.3)	47.1	28.1	8.2	5.4	4.4
PtA-HMOR30	31.0 (34.1)	32.9	15.5	8.2	9.0	3.4
PtA-HMOR45	34.3 (37.6)	34.4	11.7	6.6	8.8	4.2
PtA-HMOR90	53.1 (60.1)	21.2	5.3	4.8	11.6	4.0
PtA-HMOR120	60.1 (67.9)	14.8	5.3	5.1	11.5	3.2

[a] The percentage of isomers indicated in parentheses was calculated without considering C_8 naphthenes in the products.

Whatever the conversion, a large increase in the selectivity to xylenes can be observed when the Si/Al ratio of the zeolite component passes from 20 to 120. Thus, at 35% conversion, the selectivity in isomerization passes from 7% to 60% if all the products are considered, or from 7.5% to 68% if C_8 naphthenes, which in the isomerization unit are recycled with the C_8 aromatic cut, are not considered. This increase is due to a significant decrease in the selectivity to disproportionation products, from 47 to 15% and to dealkylation products, and from 28 to 5% (Table 4). A slight decrease in the selectivity to cracking products is also observed whereas the selectivity to transalkylation products remains practically constant.

Curiously, the selectivity to xylenes of PtA-HMOR10 and especially of PtA-HMOR6.6 is higher than the selectivity of PtA-HMOR20. This can be related to the participation in the various reactions of only the protonic sites of the shell of the crystallites owing to diffusion limitations in these mordenite samples which have practically no mesopores (7). At 35% conversion, the selectivity of PtA-HMOR6.6 ($n_{Pt}/n_{H^+} = 0.07$) is comparable to that of PtA-HMOR45, i.e., of a sample with n_{Pt}/n_{H^+} equal to 0.42. Therefore, if all the protonic sites of this latter catalyst participate in isomerization, it would be the case for only 17% ($0.07 \times 100/0.42$) of those of PtA-HMOR6.6. PtA-HMOR10 has an isomerization selectivity close to that of a sample having a Si/Al ratio between 20 and 30. Therefore, 30% of the acid sites of PtA-HMOR10 would participate in ethylbenzene isomerization. These values are greater than those calculated from the linear correlation between TOF in disproportionation and n_{H^+} and from the TOF in dealkylation. Whatever the case, it can be concluded that the particular selectivity of PtA-HMOR6.6 and −10 catalysts (Table 4B) is due to the participation in ethylbenzene transformation of only the protonic sites of the outer part of the zeolite crystallites as was previously proposed by Fernandes *et al.* (7).

CONCLUSIONS

From this comparison of the activity and selectivity of this series of $PtAl_2O_3$ (75 wt%)–mordenite (25 wt%) catalysts, the following conclusions can be drawn:

1. With all the catalysts, ethylbenzene undergoes, in addition to the desired isomerization reaction, three direct transformations: hydrogenation into C_8 naphthenes which is very limited by thermodynamic equilibrium, disproportionation, and dealkylation. Secondary reactions of transalkylation ethylbenzene–xylenes and of naphthene cracking are also observed.

2. With all the catalysts, hydrogenation and disproportionation are the fastest reactions and dealkylation is very slow; the rate of isomerization depends very much on the zeolite component. For hydrogenation, thermodynamic equilibrium is established at relatively short contact times.

3. Except for the catalysts having HMOR6.6 and −10 as acid components, the activity in disproportionation is proportional to the square of the concentration in protonic sites, which suggests the participation of two protonic sites in the bimolecular transformation; the activity in

dealkylation depends on the concentration in protonic sites and also on their acid strength; the change of the activity in ethylbenzene isomerization of the protonic sites (the turnover frequency) with the balance between the hydrogenating and acid activities is the one expected from a bifunctional mechanism.

4. The behavior of the catalysts with HMOR6.6 and −10 acid components is particular. This can be related to the absence of mesopores in the mordenite crystallites, the consequence being that acidic reactions occur only in the shell of the crystallites. The effectiveness factor for HMOR6.6 and −10 could be as low as 0.03–0.15 and 0.15–0.30, respectively.

5. The bifunctional catalysts which are the more selective in ethylbenzene isomerization are those for which the limiting step is the acid isomerization of ethylcyclohexene intermediates. This can be obtained for high values of the ratio between the concentrations of accessible Pt sites and of protonic sites accessible by reactant molecules, i. e., for bifunctional catalysts containing a very dealuminated mordenite and also for bifunctional catalysts containing mordenite without mesopores.

REFERENCES

1. Beck, J. S., and Haag, W. O., *in* "Handbook of the Heterogeneous Catalysis" (G. Ertl, H. Knözinger, and J. Weitkamp, Eds.), Vol. 5, p. 2136. VCH, Weinheim, 1997.
2. Chen, N. Y., Garwood, W. E., and Dwyer, F. G., *in* "Shape Selective Catalysis in Industrial Applications" (H. Heinemann, Ed.), Chemical Industries Vol. 36, p. 203. Dekker, New York, 1989.
3. Olson, D. H., and Haag, W. O., ACS Symposium Series 284, Chap. 14, p. 275. Am. Chem. Soc., Washington, DC, 1984.
4. Ribeiro, M. F., Travers, C., Raatz, F., Marcilly, C., and Ribeiro, F. R., *in* "Zeolites: Facts, Figures, Future" (P. A. Jacobs and R. A. van Santen, Eds.), Stud. Surf. Sci. Catal., Vol. 49, Part B, p. 1349. Elsevier, Amsterdam, 1989.
5. Alario, F., Barraqué, M., Marcilly, C., *in* "Génie des Procédés," Tome J3, p. J 5920. Techniques de l'Ingénieur, Paris, 1996.
6. Sie, S. T., de Vries, A. F., Mesters, C. M. A. M., Boon, A. Q. M., Bottenberg, K., and Trautrims, B., *Erdöl Erdgas Kohle*, November, 463 (1996).
7. Fernandes, L. D., Monteiro, J. L. F., Sousa-Aguiar, S. F., Martinez, A., Corma, A., *J. Catal.* **177**, 363 (1998).
8. Guisnet, M., *l'Actualité Chimique*, April, 9 (1989).
9. John, H. H., Neubauer, H. D., and Birke, P., *Catal. Today* **49**, 211 (1999).
10. Baraqué, M., *l'Actualité Chimique*, Octobre, 18 (1997).
11. Gonzalez, H., Rodriguez, A., Cedeno, L., Ramirez, J., and Aracil, J., *Ind. Eng. Chem. Res.* **35**, 3964 (1996).
12. Franck, H.-G., and Stadelhofer, J. W., "Industrial Aromatic Chemistry, Raw Materials, Process, Products." Springer-Verlag, Berlin, 1988.
13. Gnep, N. S., and Guisnet, M., *Bull. Soc. Chim. Fr.* **5–6**, 429 (1977).
14. Gnep, N. S., and Guisnet, M., *Bull. Soc. Chim. Fr.* **5–6**, 435 (1977).
15. Röbschläger, K. H., and Christoffel, E. G., *Ind. Eng. Chem. Prod. Res. Dev.* **18**, 347 (1979).
16. Nitta, M., and Jacobs, P., *in* "Catalysis by Zeolites" (B. Imelik, C. Naccache, Y. Ben Taarit, J. C. Vedrine, G. Coudurier, and H. Praliaud, Eds.), Stud. Surf. Sci. Catal., Vol. 5, p. 251. Elsevier, Amsterdam, 1980.
17. Hsu, Y. S., Lee, T. Y., and Hu, H. C., *Ind. Eng. Chem. Res.* **27**, 942 (1988).
18. Guisnet, M., Ayrault, P., and Datka, J., *Polish J. Chem.* **71**, 1445 (1997).
19. Guisnet, M., Ayrault, P., and Datka, J., *Polish J. Chem.* **71**, 1455 (1997).
20. Moreau, F., unpublished results.
21. Silva, J. M., Ribeiro, M. F., Ribeiro, F. R., Benazzi, E., and Guisnet, M., *Appl. Catal.* **125**, 15 (1995).
22. Stull, D. R., Westrum, E. F., and Sinke, G. C., "The Chemical Thermodynamics of Organic Compounds." Wiley, New York, 1969.
23. Koeding, W. W., *J. Catal.* **95**, 512 (1985).
24. Morin, S., Gnep, N. S., and Guisnet, M., *J. Catal.* **159**, 296 (1996).
25. Guisnet, M., Avendano, F., Bearez, C., and Chevalier, F., *J. Chem. Soc., Chem. Commun.* 336 (1985).
26. Guisnet, M., *Acc. Chem. Res.* **23**, 392 (1990).
27. Karge, H. G., Ladebeck, J., Sarbak, Z., and Hatada, K., *Zeolites* **2**, 94 (1982).
28. Amelse, J. A., *in* "Proceeding, 10th North American Meeting of the Catalyst Society" (J. Ward, Ed.), Stud. Surf. Sci. Catal., Vol. 38, p. 165. 1988.
29. Silva, J. M., Ribeiro, M. F., Ribeiro, F. R., Benazzi, E., and Guisnet, M., *Appl. Catal.* **125**, 1 (1995).
30. Gnep, N. S., Roger, P., Cartraud, P., Guisnet, M., Juguin, B., and Hamon, C., *C. R. Acad. Sci. Paris, Série II*, **309**, 1743 (1989).
31. Meima, G. R., van der Aalst, M. J. M., Samson, M. S. V., Garces, J. M., and Lee, J. G., *in* "Proceedings, 9th International Zeolite Conference" (R. van Ballmoos, J. B. Higgins, and M. M. J. Treacy, Eds.), Vol. II, p. 327. Butterworths Heinemann, Boston, 1992.
32. Weitkamp, J., *Ind. Eng. Chem. Prod. Res. Dev.* **21**, 550 (1982).
33. Guisnet, M., and Pérot, G., *in* "Zeolites: Science and Technology" (F. R. Ribeiro, A. E. Rodrigues, L. D. Rollmann, and C. Naccache, Eds.), NATO Series E, Vol. 80, p. 397. Martinus Nijhoff, The Hague, 1984.
34. Weitkamp, J., and Ernst, S., *in* "Guidelines for Mastering Properties of Molecular Sieves. Relationship between the Physicochemical Properties of Zeolitic Systems and Their Low Dimensionality" (D. Barthomeuf, E. G. Derouane, and W. Hölderich, Eds.), NATO ASI Series B, Vol. 221, p. 343. Plenum, New York, 1990.
35. Guisnet, M., Alvarez, F., Giannetto, G., and Pérot, G., *Catal. Today* **1**, 415 (1987).
36. Alvarez, F., Ribeiro, F. R., Pérot, G., Thomazeau, C., and Guisnet, M., *J. Catal.* **162**, 179 (1996).